RETRIEVING COASTAL SEA SURFACE TEMPERATURE FROM LANDSAT-8 TIRS FOR WANGI-WANGI ISLAND, WAKATOBI, SOUTHEAST SULAWESI, INDONESIA

Eko Susilo*, Rizki Hanintyo, and Adi Wijaya
Institute for Marine Research and Observation
Jl. Baru Perancak, Kabupaten Jembrana, Bali 82251, Indonesia
*E-mail: ekosusilo@live.com

Received: 12 November 2018; Revised: 9 August 2019; Approved: 18 August 2019

Abstract. The new Landsat generation, Landsat-8, is equipped with two bands of thermal infrared sensors (TIRS). The presence of two bands provides for improved determination of sea surface temperature (SST) compared to existing products. Due to its high spatial resolution, it is suitable for coastal zone monitoring. However, there are still significant challenges in converting radiance measurements to SST, resulting from the limitations of in-situ measurements. Several studies into developing SST algorithms in Indonesia waters have provided good performance. Unfortunately, however, they have used a single-band windows approach, and a split-windows approach has yet to be reported. In this study, we investigate both single-band and split-window algorithms for retrieving SST maps in the coastal zone of Wangi-Wangi Island, Wakatobi, Southeast Sulawesi, Indonesia. Landsat-8 imagery was acquired on February 26, 2016 (01: 51: 44.14UTC) at position path 111 and and row 64. On the same day, in-situ SST was measured by using Portable Multiparameter Water Quality Checker – 24. We used the coefficient of correlation (r) and root mean square error (RMSE) to determine the best algorithm performance by incorporating in-situ data and the estimated SST map. The results showed that there were differences in brightness temperature retrieved from TIRS band10 and band 11. The single-band algorithm based on band 10 for Poteran Island clearly showed superior performance (r = 69.28% and RMSE = 0.7690°C). This study shows that the split-window algorithm has not yet produced a accurate result for the study area.

Keywords: *Landsat-8, single-band algorithm, split-window algorithm*

1 INTRODUCTION

Landsat is a joint programme between the National Aeronautics and Space Administration (NASA) and the US Geological Survey (USGS). The most recent satellite, Landsat 8 (Landsat Data Continuity Mission, LDCM), was launched successfully on February 11, 2013. The satellite records a 185-km swath in a sun-synchronous orbit at an altitude of 705 km, repeated every 16 days. There are two main sensors onboard Landsat 8, the Operational Land Imager (OLI) and the Thermal Infrared Sensor (TIRS). OLI collects images from 9 bands at wavelengths ranging from 0.43 µm to 2.30 µm at 30-metre (multispectral) and 15-metre (panchromatic) spatial resolutions. TIRS collects thermal images with a 100-metre spatial resolution for two bands ranging from 10.30 µm to 12.50 µm. To meet the 30-metre native resolution of OLI, the TIRS bands are resampled by cubic convolution (Irons et al., 2012; Roy et al., 2014).

The current SST map products such as Aqua/Terra MODIS and Suomi-NPP VIIRS have limitations in their ability to address oceanographic phenomena in

http://dx.doi.org/10.30536/j.ijreses.2019.v16.a3044

coastal waters, while Landsat 8 has better capabilities than these previous-generation products. Due to its high spatial resolution, it is suitable for monitoring coastal zones. The presence of two TIRS bands onboard Landsat-8 also opens up improved opportunities for determination of sea surface temperature (SST) compared to existing products, especially in coastal waters (Irons et al., 2012; Jimenez-Munoz, Sobrino, Skokovic, & Mattar, 2014; Roy et al., 2014). Landsat 8 could produce more detailed SST maps in the coastal waters up to 100 metres and so could observe coastal water dynamics such us thermal fronts and SST change in coral reef ecosystems or marine aquaculture areas. However, there are still significant challenges related to both the conversion of radiance algorithms and the limitations of in-situ measurements (Fisher & Mustard, 2004; Thomas, Byrne, & Weatherbee, 2002). Several research activities have been tried to develop appropriate algorithms to generate SST maps from Landsat 8 TIRS. Generally, these algorithms can be divided into two methods: (1) single-band algorithms and (2) split-window algorithms. Single-band algorithms have been widely used to determine SST from data provided by previous Landsat TM and ETM+ (Fisher & Mustard, 2004; Thomas et al., 2002; Trisakti, Sulma & Budhiman, 2004; Xing, Chen, & Shi, 2006). In Indonesia, single-band algorithms for TIRS were first introduced by Arief, Adawiah, Parwati, Hamzah, & Prayogo, (2015) and Syariz et al. (2015), both of which perform well. The split-window algorithm can be applied for all sensors with at least two thermal bands (such as AVHRR and MODIS). Since TIRS bands are split into two spectral bands, the split-window method can be applied (Jimenez-Munoz et al., 2014; Xufeng et al., 2015).

No operational Landsat 8 TIRS algorithms have been published either for single or multi-band windows. In this present study, we investigate both single-band and split-window algorithms for retrieving SST maps for the coastal waters of Wangi-Wangi Island, Wakatobi, Southeast Sulawesi, Indonesia.

2 MATERIALS AND METHODOLOGY

2.1 Landsat 8 imagery

Wangi-Wangi Island is one of the islands in the Wakatobi National Park, Southeast Sulawesi. Located in the Coral Triangle, this park has various types of coral and other reef biota spread across 25 pieces of coral reef along the 600 km coastline.

Landsat 8 imagery was acquired on February 26, 2016 (01: 51: 44.14UTC) at path position 111 and row position 64. The Level-1 product was downloaded from the US Geological Survey (http://earthexplorer.usgs.gov).

2.2 In-situ SST

In-situ sea surface temperature observations (SST obs) were obtained at 7 sampling stations in the southern part of Wangi-Wangi Island, Wakatobi (Figure 2-1). The measurement time coincided with the Landsat 8 satellite passing time at 2 hours before and 2 hour after passing time, and was carried out using Portable Multiparameter Water Quality Checker - 24. These tools use 'thin-film platinum resistance' sensors and can measure temperature ranging from -5°C to 55°C within an error range of 0.25°C. SST measurement was repeated 3 times for each sampling station to minimize error and SST obs value was calculated based on the average of the three measurements.

2.3 TIRS data processing

The Level-1 terrain-corrected (L1T)

product has been radiometrically and geometrically corrected as defined in the Universal Transverse Mercator (UTM) map projection with World Geodetic System 84 (WGS84) datum. Complete L1T consists of 9 files corresponding to the OLI bands (1–9) and 2 files corresponding to the TIRS bands (10 and 11). A spatially explicit data-quality assessment that indicates the probability of clouds is also provided, known as the quality assessment (QA) band.

TIRS band values in digital numbers (DNs) are reconverted to the quantity which reflects sea surface heat-radiation characteristics of the pixel-level spectral data according to Formula 2-1, while the brightness temperature (T in K) from both TIRS bands was computed based on spectral radiance following Formula 2-2:

$$L_\lambda = M_L \text{ x } Q_{cal} + A_L \qquad (2\text{-}1)$$

$$T = \frac{K_2}{ln\left(\frac{K_1}{L_\lambda}+1\right)} \qquad (2\text{-}2)$$

In these formulae, L_λ is the spectral radiance (W m - 2sr - 1µm - 1), M_L is a radiance multiplicative scaling factor for each band, A_L is a radiance additive scaling factor for each band, Q_{cal} is DNs value, and K_1 and K_2 are thermal conversion constants for each band (USGS 2015).

TIRS scaling factor and thermal conversion constants are listed in Table 2-1. To reduce the effect of cloud problems, we used a band quality assessment (BQA) on Landsat 8 to indicate cloud masking (USGS, 2015).

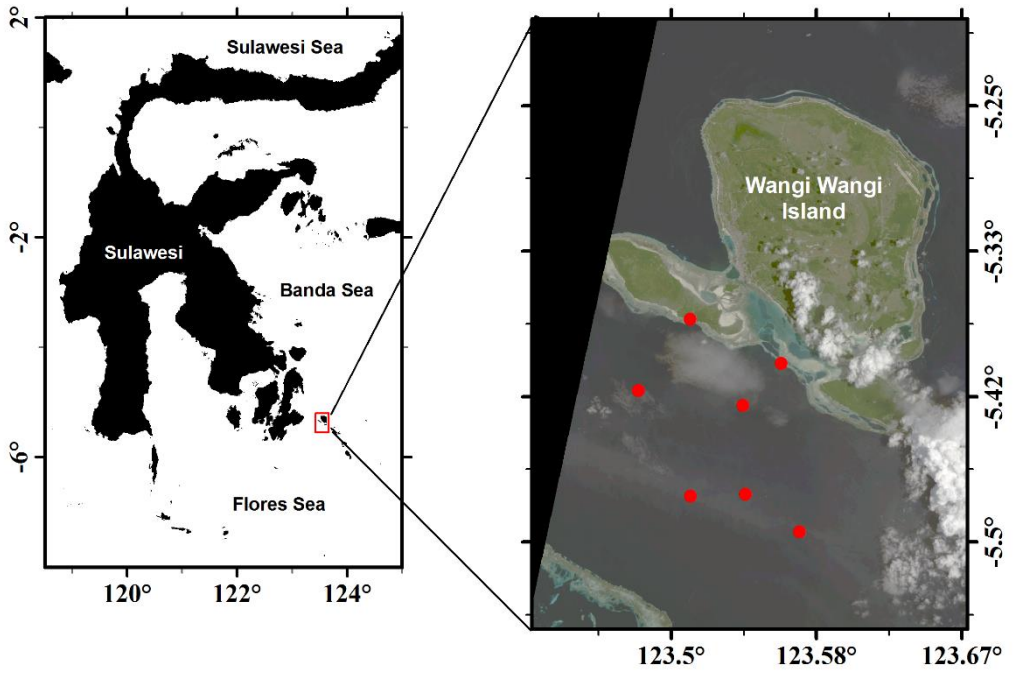

Figure 2-1: Natural colour imagery of Wangi-Wangi Island waters from Landsat 8 acquired on February 26, 2016, with red dots (●) representing the sites of the in-situ SST from 7 stations.

Table 2-1: TIRS scaling factor and thermal conversion constant.

Band	M_L	A_L	K_1	K_2
B_{10}	0.0003342	0.1	774.8853	1321.0789
B_{11}	0.0003342	0.1	480.8883	1201.1440

3 RESULTS AND DISCUSSION

3.1 In-situ SST

Coinciding with Landsat 8 satellite passing time (09:51 WITA), in-situ SST were carried out to the south of Wangi-Wangi Island. Due to time limits, we were only able to collect data from 7 stations during this survey campaign (Table 3-1). SST obs were repeated 3 times for each sampling station to minimize error. Furthermore, SST obs value was calculated based on the average of the three measurements. The results indicate that SST obs during Landsat 8 passage tend to be homogeneous, with a mean of 29.86°C and standard error of 0.065°C indicating that warm water is found around this site.

The Landsat 8 temporal resolution is 16 days. It would therefore have been better if we could have collected SST obs every 16 days at the same places to create a long time series in-situ dataset.

3.2 Brightness temperature

The brightness temperature was calculated according to Formula 2. This value represents the effective temperature viewed by the satellite under an assumption of unity emissivity (Figure 3-1). Generally, there are significant differences between the two Landsat TIRS bands (*DT = T10 - T11*) ranging from 0–10K. A previous study in Indonesia waters also showed this but with a lower value, the mean brightness temperature deviation in Lampung Bay being 1–1.5°C (Arief et al., 2015). TIRS bands work in different long-wave infrared (LWIR) wavelengths: band 10 (10.60–11.19μm) and band 11 (11.50–12.51μm). In comparison with NOAA, AVHRR and MODIS sensors, these bands had almost the same characteristics as band 4 (10.30–11.30μm) and band 5 (11.50–12.50μm) for the AVHRR sensor and band 31 (10.78–11.28μm) and band 32 (11.77–12.27μm), where NOAA, AVHRR and MODIS had been widely used for retrieving SST data.

Spectral characteristics led band-10 produce a higher brightness temperature value than band 11. This could be because of the blackbody radiation theory, known as Planck's law curves. On the earth's surface, the highest spectral radiant emittance occurs at around 10 μm and this might be the reason band 10 of Landsat 8 had higher brightness temperature than band 11. The availability of two separate bands can reduce error in the retrieval of surface temperature in comparison to previous Landsat data (TM and ETM+). Although there were two thermal bands on Landsat TM and ETM+, the fact that both thermal bands work on the same wavelength but in different gain-setting sensors resulted in different brightness temperature information.

Table 3-1: In-situ sea surface temperature (SST obs) dataset.

Station	Time (WITA)	Latitude	Longitude	SST obs (°C)
1	08:12	-5.4132	123.4812	29.8
2	09:17	-5.4737	123.5113	29.9
3	09:53	-5.4726	123.5427	30.0
4	10:06	-5.4217	123.5410	29.9
5	10:27	-5.3723	123.5109	29.6
6	10:50	-5.3976	123.5632	29.7
7	11:03	-5.4941	123.5738	30.1

The differences in the brightness temperature from 7 sampling stations in Wangi-Wangi coastal waters range between 3 and 5°K (Figure 3-1). Of the stations, 5 had a temperature higher than 3.5°K, and only 2 had temperature of less than 3.5°K. Those 2 stations were located on the edge of the TIRS dataset, but it is uncertain whether station location could lead to the lower deviation among these bands.

The cloud-masking technique using BQA value did not provide a completely cloud-free image, but cloud and cirrus features can be masked well by BQA. The Landsat 8 BQA classification is defined by cloud cover assessment (CCA) algorithms. At launch, there are four CCA algorithms: ACCA, See-5 CAA, Cirrus CCA, and AT-ACCA (USGS, 2015). However, we obtained data for several areas which were covered by haze, especially in the southern parts of Wangi-Wangi Island. This haze also appeared on the edge of cloud features. Based on Figure 3-1, we could assume that the brightness temperature values of less than 291K (band 10) or less than 288K (band 11) could be classified as haze. Zhang, Guindon, and Cihlar, (2002) defined haze as spatially varying, semi-transparent cloud and/or aerosol layers on an image. Both cloud and haze had a similar effect in increasing the radiometric (DNs) values. Unfortunately, there is no operational algorithm available yet to minimize haze contamination on Landsat 8 imagery. The Landsat 8 science team is still working on this and will add an algorithm to deal with haze in the future.

3.3 Algorithm evaluation

In this present study, we investigated single-band algorithms developed in two different areas: Poteran Island (Syariz et al., 2015) and Lampung Bay (Arief et al., 2015). We also investigated two different split-window algorithms: open sea NOAA MCSST algorithm (Walton, Pichel, Sapper, & May, 1998) and regional MCSST algorithm in the South China Sea (Xufeng et al., 2015). Equation formulae for each algorithm investigated in the present study are listed in Table 3-2.

To evaluate the relationship of the estimated SST and the SST obs, the brightness temperature for each TIRS band was extracted and calculated from the average at 9-pixel values surrounding the sampling station. This technique can reduce the influence of noise and minimize inaccuracy in determining the location of GPS tools (Hansen, Williams, & Adjei, 2015). The 9 pixels average resulted in 270-metre pixel size. In fact, the TIRS bands were acquired at 100-metre resolution but were resampled to 30 metres to obtain the same resolution as the OLI bands. The averaged pixels had twice larger than originally related to thermal emissivity information.

The analysis results of the evaluation showed that there was a different response for each single-window algorithm compared to the SST obs. The single-window algorithm from band 11 was more accurate than for band 10 for both Poteran Island and Lampung Bay. These results had the same pattern in both locations (Arief et al., 2015; Syariz et al., 2015). This study obtained Pearson's correlation coefficients for both algorithms, of 74.53 and 64.94, respectively. Both still had high root mean square error (RMSE) values of 1.2939°C and 3.4790°C, respectively. The lowest RMSE values were produced by the single-window algorithm from band 10, at 0.7690°C and 0.2713°C, respectively. Unfortunately, the lowest RMSE value did not coincide with a high correlation coefficient. Generally, the quadratic polynomial model (Poteran Island) had

better spatial performance than the cubic polynomial model used in Lampung Bay.

Visually, the first 3 algorithms (SST1, SST2, and SST3) provided a mismatch of SST interpretations. Higher SST was observed in the area which was suspected to be covered by haze. We found 3 large areas with haze features in the northern and southern parts of the island (Figure 3-1). On the other hand, lower SST was observed in the areas adjacent to the land. Different issues were demonstrated by the SST4 algorithm; it could identify the area suspected as being hazy with low SST values.

The open ocean split-window algorithm (SST5) provided a better spatial SST result than for the South China Sea waters and also for the 4 previous single-band algorithms. This algorithm was first advanced based on the fourth and fifth bands of NOAA/AVHRR. These two bands had a similar wavelength spectrum as TIRS Landsat 8 (10.3-11.3μm and 11.5-12.5μm). Unfortunately, SST5 had a low Pearson correlation value and higher RMSE value (overestimate). SST6 had been developed in a temperate region and was not suitable for tropical areas, as evidenced by a worse result than the other algorithms.

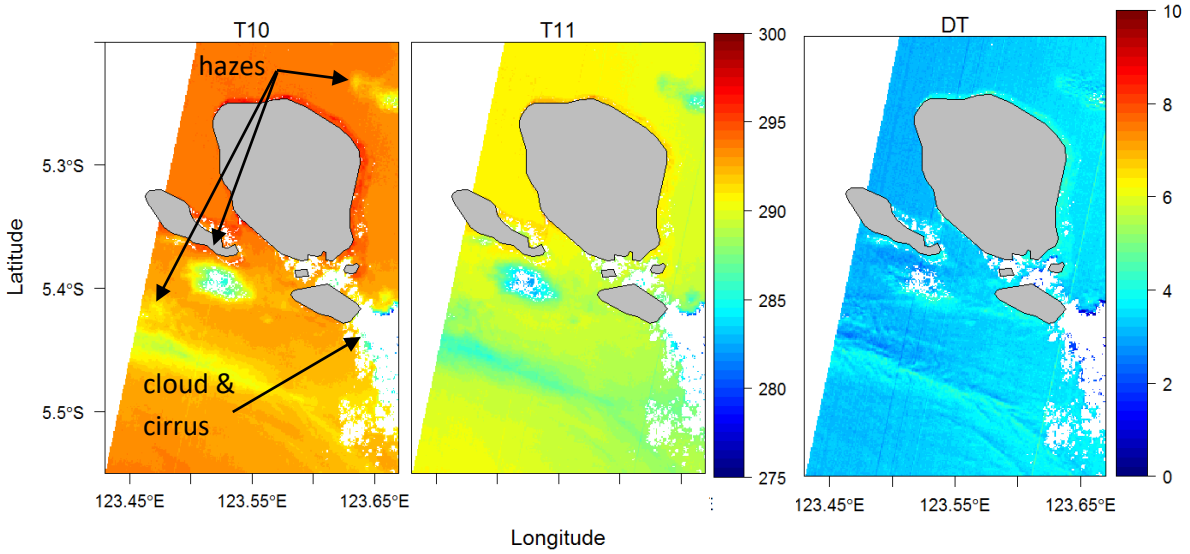

Figure 3-1: Brightness temperature deviation among TIRS bands in Wangi-Wangi Island coastal waters on February 26, 2016.

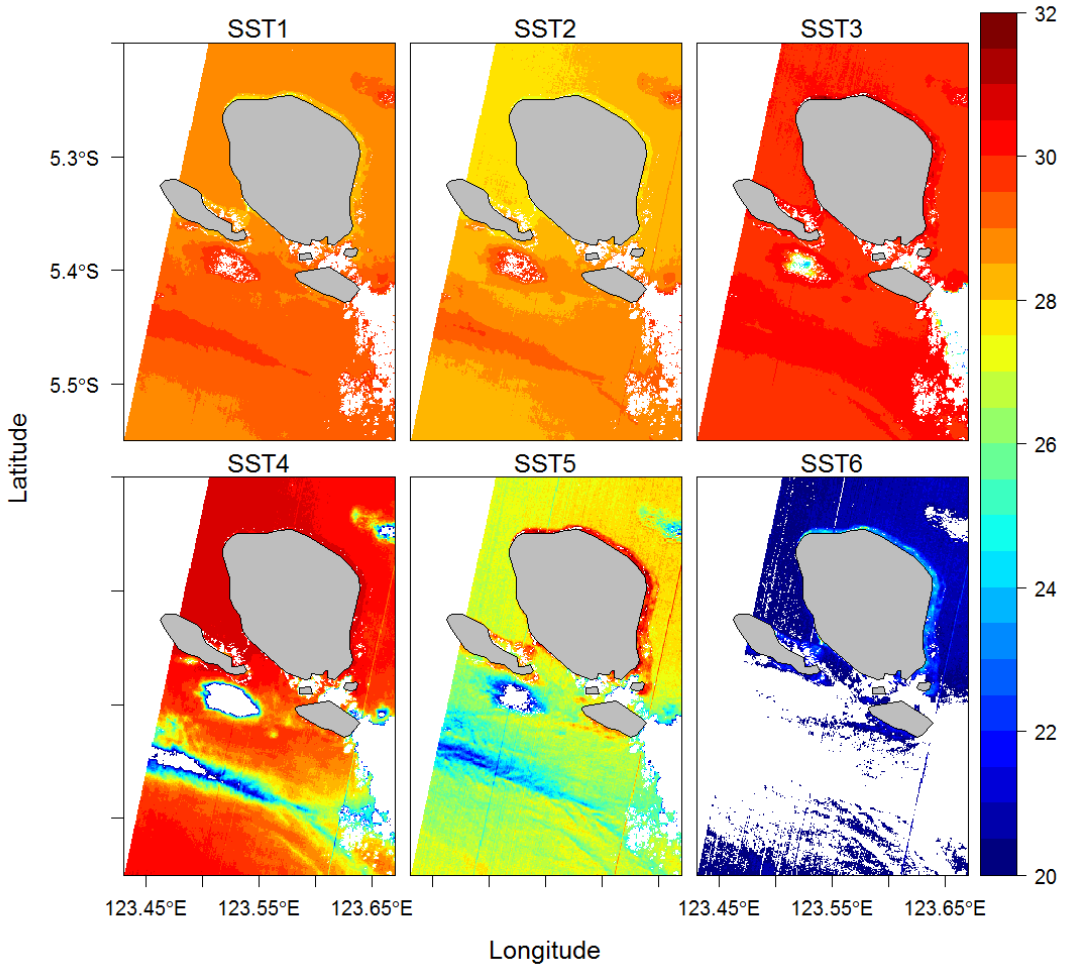

Figure 3-2: Estimated SST from different algorithms in Wangi-Wangi Island coastal waters on February 26, 2016.

Table 3-2: The algorithms investigated.

Formula	Location
$SST1 = -0.0273 \times (T_{10} - 273.15)^2 + 0.7474 \times (T_{10} - 273.15) + 24.882$	Poteran Island, Indonesia
$SST2 = -0.0197 \times (T_{11} - 273.15)^2 + 0.2881 \times (T_{11} - 273.15) + 29.004$	
$SST3 = 0.0234 \times (T_{10} - 273.15)^3 - 1.3107 \times (T_{10} - 273.15)^2 + 24.335 \times (T_{10} - 273.15) - 119.68$	Lampung Bay, Indonesia
$SST4 = 0.0597x (T_{11} - 273.15)^3 - 3.4178 \times (T_{11} - 273.15)^2 + 65.056 \times (T_{11} - 273.15) - 381.21$	
$SST5 = 1.0222 \times T_{10} + 2.31 \times (T_{10} - T_{11}) - 280.39 + 0.83 \times (T_{10} - T_{11}) \times (sec\theta - 1)$	Open ocean
$SST6 = 0.998 \times T_{10} + 1.89 \times (T_{10} - T_{11}) - 278.74 + 0.72 \times (T_{10} - T_{11}) \times (sec\theta - 1)$	South China Sea

Where SST is sea surface temperature (°C), T_{10} and T_{11} are the brightness temperature measured by TIRS (K), and θ is the sensor zenith angle (degree)

Table 3-3: Summary of the algorithm evaluation criteria.

Algorithm	SST1	SST2	SST3	SST4	SST5	SST6
r	69.28	74.53	32.34	-64.94	-32.68	-40.21
RMSE	0.7690	1.2939	0.2713	3.4790	3.8666	11.2179

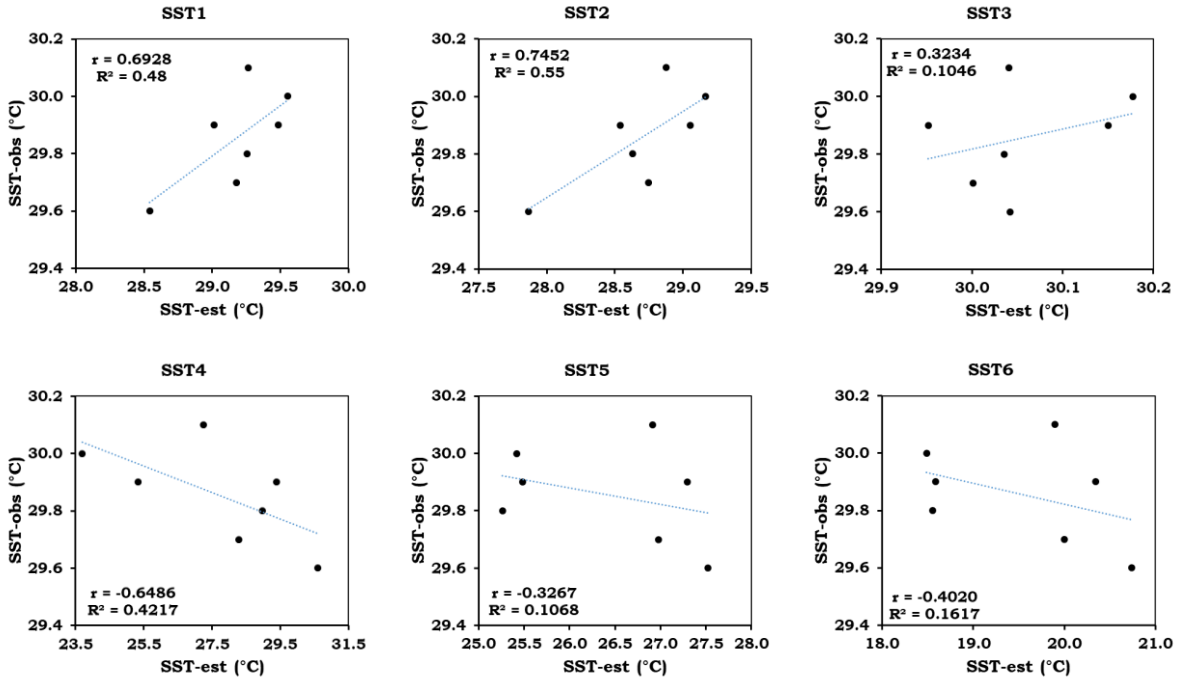

Figure 3-3: Scatter plot between the in-situ SST (SST obs) and estimated SST (SST-est) for each algorithm.

The matchup analysis showed a different response for each single-windows algorithm (Figure 3-3). In general, the quadratic polynomial model used for Poteran Island (SST1 and SST2) has better spatial performance than the cubic polynomial model used in Lampung Bay (SST3 and SST4) and the split-window algorithms (SST5 and SST6). But both still had a high RMSE value, of 0.769°C and 1.294°C, respectively.

The single-window algorithm from band 10 has a better performance than band 11. Pearson's correlation coefficient and RMSE value for SST1 are 0.69 and 0.769, respectively. This is a different pattern from the previous study at Poteran Island, in which band 11 had better performance than band 10. The SST2 algorithm gives better performance, with higher R^2 and lower RMSE with R^2 of 0.91 and the RMSE of 0.028 (Syariz et al., 2015). The lower Pearson's correlation coefficient and higher RMSE in this study are most likely caused by the lower number of SST obs.

The single-band windows for Lampung Bay Pearson's correlation coefficient for SST4 algorithm is also higher than SST3. These results differ from previous studies, in which band 10 has better performance than band 11 (Arief et al., 2015). However, the negative Pearson's correlation coefficient from both algorithms indicates they are not suitable for this site. The different layer of SST obs used in this study may contribute to this result. Both algorithms were developed by using sub-surface SST at 30-metre depth, while the analysis uses surface SST datasets.

The open ocean split-window algorithm (SST5) gives better spatial SST features than for the South China Seas waters (SST6) and also the 4 previous single-band algorithms. The spatial distribution of estimated SST (SST-est) produced by the first 3 single-band algorithms (SST1, SST2 and SST3) looks strange. The higher SST-est was observed in the area suspected of being covered by haze. There are 2 large areas with haze features surrounding this site. On the other hand, lower SST was observed in the areas adjacent to the land (Figure 3-1). Different things are demonstrated by the SST4 algorithm: it can identify the area suspected as being hazy with low SST values in addition to SST5.

Unfortunately, SST5 and SST6 have low Pearson correlation values and higher RMSE values (overestimates). The SST5 algorithm was first advanced based on the fourth and fifth bands of NOAA/AVHRR. These 2 bands have a similar wavelength spectrum to TIRS Landsat 8 (10.3–11.3μm and 11.5–12.5μm). Most were developed based on data from drifting and moored buoys in the tropical Pacific. Meanwhile, the SST6 algorithm was developed for a temperate region and is not suitable for tropical areas, as evidenced by its giving a worse result than the other algorithms. There need to be some adjustments in order to apply this global algorithm to a local area.

4 CONCLUSION

Each algorithm could retrieve SST data in particular coastal water as well as in the entire global area. However, there is still a performance gap in implementing them across different areas in which each has its own environmental characteristics. The single-band algorithm based on band 10 used in Poteran Island had the best performance, with the highest coefficient of correlation value (r = 69.28%) and the lowest RMSE value (RMSE = 0.7690°C). However the split-window algorithm does not give a better result in describing the SST estimation for the study area.

ACKNOWLEDGMENTS

The present study was funded in 2016 by the Ministry of Marine Affairs and Fisheries, the Republic of Indonesia, through the Institute for Marine Research and Observation (IMRO). The authors wish to thank the US Geological Survey for providing Landsat 8 data freely and the Institute for Marine Engineering and Technology, Wakatobi, for providing a ship for conducting the in-situ measurements. We also express our appreciation to Dr Bambang Sukresno, M.Si. and Dr I Nyoman Radiarta, M.Sc., as well as to the journal editorial team and reviewer for their valuable comments.

REFERENCES

Arief, M., Adawiah, S. W., Parwati, E., Hamzah, R., & Prayogo, T. (2015). Development model of sea surface temperature extraction using Landsat- 8 satellite data, case study: Lampung Bay. *Jurnal Penginderaan Jauh*, *12*, 107–122.

Fisher, J. I., & Mustard, J. F. (2004). High spatial resolution sea surface climatology from Landsat thermal infrared data. *Remote Sensing of Environment*, *90*, 293–307.

Hansen, C. H., Williams, G. P., & Adjei, Z., (2015). Long-term application of remote sensing chlorophyll detection models: Jordanelle Reservoir case study. *Natural Resources*, *6*, 123–129.

Irons, J. R., Dwyer, J. L, & Barsi, J. A. (2012). The next Landsat satellite: The Landsat Data Continuity Mission. *Remote Sensing of Environment*, *122*, 11-21.

Jimenez-Munoz, J. C., Sobrino, J. A, Skokovic, D., & Mattar, C. (2014). Land surface temperature retrieval methods from Landsat-8 thermal infrared sensor data.

IEEE Geoscience and Remote Sensing Letters, *11*, 1840-1843.

Roy, D. P., Wulder, M. A., Loveland, T.R., Woodcock, C.E., Allen, R.G., Anderson, M. C., … Zhu, Z. (2014). Landsat-8: Science and product vision for terrestrial global change research. *Remote Sensing of Environment, 145*, 154-172.

Syariz, M. A., Jaelani, L. M., Subehi L., Pamungkas, A., Koenhardono, E. S., & Sulisetyono, A. (2015). Retrieval of sea surface temperature over Poteran Island water of Indonesia with Landsat 8 TIRS Image: A preliminary algorithm. In: *The International Archives of the Photogrammetry, Remote Sensing and Spatial Information Sciences,* (pp. 87–90).

Thomas, A., Byrne, D., & Weatherbee, R. (2002). Coastal sea surface temperature variability from Landsat infrared data. *Remote Sensing of Environment*, *81*, 262–272.

Trisakti, B., Sulma, S., & Budhiman, S. (2004). Study of sea surface temperature (SST) using Landsat-7 ETM (In Comparison with sea surface temperature of NOAA-12 AVHRR). In Liu C-T (Ed.) *Thirteenth Workshop of OMISAR (WOM-13) on validation and application of satellite data for marine resources conservation*. Bali, Indonesia: Environmental Protection Administration

Walton, C. C., Pichel, W. G., Sapper, J. F, and May, D. A. (1998). The development and operational application of nonlinear algorithms for the measurement of sea surface temperatures with the NOAA polar-orbiting environmental satellites. *Journal of Geophysical Research: Oceans*, *103*, 27999–28012.

Xing, Q., Chen, C.-Q., & Shi, P. (2006). Method of integrating landsat-5 and landsat-7 data to retrieve sea surface temperature in coastal waters on the basis of local empirical algorithm. *Ocean Science Journal, 41*, 97–104.

Xufeng, X., Yang, L., Wentong, D., Zhonglin, W., Lianlong, Z., Zhen, S., & Huang, M. (2015). An algorithm to inverse sea surface temperatures at offshore water by employing Landsat 8/TIRS Data. In A.M. Lagmay (Ed.), *36th Asian Conference on Remote Sensing 2015 (ACRS 2015): Fostering Resilient Growth in Asia Philippines:* Curran Associates, Inc, pp. 4504–4511.

Zhang, Y., Guindon, B., & Cihlar, J. (2002). An image transform to characterize and compensate for spatial variations in thin cloud contamination of Landsat images. *Remote Sensing of Environment, 82*, 173–187.